

Ordered graphitic microfoams via shrinkage and catalytic conversion of polymer scaffolds

Cite as: APL Mater. **8**, 021106 (2020); <https://doi.org/10.1063/1.5136235>

Submitted: 11 November 2019 . Accepted: 26 January 2020 . Published Online: 06 February 2020

Kenichi Nakanishi , and Stephan Hofmann 



View Online



Export Citation



CrossMark

ARTICLES YOU MAY BE INTERESTED IN

[Polymer-perovskite blend light-emitting diodes using a self-compensated heavily doped polymeric anode](#)

APL Materials **8**, 021101 (2020); <https://doi.org/10.1063/1.5140519>

[Signatures of temperature driven antiferromagnetic transition in the electronic structure of topological insulator \$\text{MnBi}_2\text{Te}_4\$](#)

APL Materials **8**, 021105 (2020); <https://doi.org/10.1063/1.5142846>

[Mechanism of Mn emission: Energy transfer vs charge transfer dynamics in Mn-doped quantum dots](#)

APL Materials **8**, 020901 (2020); <https://doi.org/10.1063/1.5140888>

ORDER PRINT EDITION



AIP Conference Proceedings

**The 18th International Conference
on Positron Annihilation**

Ordered graphitic microfoams via shrinkage and catalytic conversion of polymer scaffolds

Cite as: APL Mater. 8, 021106 (2020); doi: 10.1063/1.5136235
Submitted: 11 November 2019 • Accepted: 26 January 2020 •
Published Online: 6 February 2020



Kenichi Nakanishi  and Stephan Hofmann ^{a)} 

AFFILIATIONS

Department of Engineering, University of Cambridge, J. J. Thomson Avenue, Cambridge CB3 0FA, United Kingdom

^{a)} Author to whom correspondence should be addressed: sh315@cam.ac.uk

ABSTRACT

Carbon foams are a highly attractive class of low-density materials whose structural, electrical, thermal, and chemical properties are strongly linked to the level of graphitization and 3D structure. Pyrolytic graphitization requires very high temperatures (>2000 °C), and most current graphitic foams are stochastically arranged with restricted control over pore size and architecture. We report on the shrinkage and catalytic conversion of commercial polymer foams and 3D printed templates as a facile, cost-effective method to scalably reach and control sub-200 μm unit cell sizes and a high level of graphitization at temperatures below 1100 °C. We demonstrate the conversion of 3D printed cubic polymer lattices to an identically shaped carbonaceous network with shrinkage controlled via an atomic layer deposited oxide coating up to a maximum 125 fold decrease in volume and over 95% mass loss through slow carbonization. This is accompanied by a reduction in the unit cell size from 1000 μm to 170 μm and strut widths from 550 μm to 65 μm. The structures are subsequently coated with a sacrificial metal catalyst by electroless deposition to achieve efficient graphitization while maintaining structural order. We discuss the underlying mechanisms and opportunities to tailor the processes and structure to manifold application needs.

© 2020 Author(s). All article content, except where otherwise noted, is licensed under a Creative Commons Attribution (CC BY) license (<http://creativecommons.org/licenses/by/4.0/>). <https://doi.org/10.1063/1.5136235>

Lightweight three-dimensionally (3D) ordered carbon foams are in ever increasing demand for applications ranging from thermal management¹ and mechanical metamaterials² to (bio)sensors,³ filtration,⁴ electromagnetic shielding,⁵ and energy storage.⁶ The physical and chemical properties of such foams strongly depend on both the constituent carbon and the foam structure. With the rise of graphene, a focus of the recent literature has been to achieve a high level of graphitization to endow the foam with the unique properties of 2D materials, such as an enhanced electrical⁷ or thermal⁸ conductivity. Pyrolytic graphitization requires very high temperatures, and this motivates catalytic approaches which have been demonstrated using many different carbon precursors including gaseous hydrocarbons as part of a chemical vapor deposition process (CVD) or solid carbon precursors such as polymers,⁹ biomass,¹⁰ and recycled carbon.¹¹ A key challenge to such manufacturing approaches is 3D catalyst/precursor templating, specifically combining scalability and structural control down to the micrometer-scale and below. The use of commercial foams, dealloying, or powder sintering methods does not allow for ordered template design, while approaches like 2-photon lithography or co-block polymer self-assembly currently

lack scalability and throughput. An appealing approach to overcome this challenge is to 3D pattern at an easily implementable larger size scale and to subsequently shrink the template while preserving its geometry. Pyrolytic shrinkage has been previously demonstrated with both bulk foamed polymers¹² and photopolymers² used in 2-photon direct laser writing (2P-DLW). Such a pyrolysis process results in the removal of the bulk side-chain species, leaving behind a disordered carbon allotrope primarily composed of sp²-bonded carbon.¹³ A typical reduction in volume of 75% can thereby be achieved¹⁴ down to unit cell sizes of 1 μm. However, the lateral dimensions of 2P-DLW fabricated lattices are limited to hundreds of micrometers. Self-propagating photopolymer waveguides can be used to scalably produce and shrink micro-lattice architectures across a range of interconnected patterns.¹⁵ The resulting pyrolytic carbon materials, however, remain non-conductive for all these methods.

Here, we explore the combination of pyrolytic shrinkage of commercial 3D patterned polymeric templates with catalytic graphitization as a facile, cost-effective method to scalably reach and control sub-200 μm unit cell-sized graphitic foams. We show that the

degree of isotropic template shrinkage and surface wrinkling can be controlled by the addition of a conformal atomic layer deposited (ALD) oxide coating applied prior to carbonization. We demonstrate the conversion of 3D printed cubic polymer lattices to an identically shaped carbonaceous network up to a 125 fold decrease in volume and over 95% mass loss through slow carbonization. This is accompanied by a reduction in the unit cell size from $1000\ \mu\text{m}$ to $170\ \mu\text{m}$ and strut widths from $550\ \mu\text{m}$ to $65\ \mu\text{m}$. We employ a conformal, sacrificial coating with a transition metal catalyst via electroless deposition to achieve efficient graphitization as highlighted by Raman spectroscopy while maintaining structural order. We discuss the underlying mechanisms and opportunities to tailor the processes and structure to manifold application needs.

Melamine foams are cheaply available, possessing a low density ($\sim 8\ \text{mg}/\text{cm}^3$) and high porosity ($>99\%$), motivating their use as a polymeric template. Prior literature on carbonization (N_2 , 1 atm, $1000\ ^\circ\text{C}$) of melamine foams demonstrated non-conductive carbon foams with $4\times$ shrinkage that remained elastic under compression up to 80% .¹² The synthesis scheme used herein for the pyrolytic shrinkage of commercial melamine foam to form a carbon network (CN) is shown in Fig. 1(a), along with scanning electron microscopy (SEM) images at each step of the process. Foam samples were cleaned and then subjected to a slow pyrolytic carbonization process in an inert argon atmosphere (250 mbar, 200 sccm). Samples were ramped to $350\ ^\circ\text{C}$ at a rate of $3\ ^\circ\text{C}/\text{min}$, held for 30 min, and then further ramped to $450\ ^\circ\text{C}$ at a rate of $5\ ^\circ\text{C}/\text{min}$ and held

for additional 60 min. The slow rate of degassing and decomposition enabled isotropic shrinkage with an $8\times$ decrease in volume and approximately 50% mass loss. The increased level of shrinkage is attributed to the reduced pressure used during the carbonization process, which encouraged the release of N-containing gases and more thorough carbonization. Raman spectra were measured at RT using a Renishaw inVia spectrometer at 532 nm excitation with $20\times$ and $50\times$ objectives. Figure 1(b) shows the characteristic Raman spectra of the untreated melamine resin.¹⁶ An explicit strong peak at $\nu \approx 980\text{--}990\ \text{cm}^{-1}$ is a signature of all melamine-containing compounds, arising from a triazine ring breathing mode. A set of peaks around $\nu = 1250\text{--}1600\ \text{cm}^{-1}$ is mainly ascribed to vibrations of N-CH₂-O groups, while the peak at $\nu = 2960\ \text{cm}^{-1}$ is associated with C-H stretching vibrations in the formaldehyde part of the resin. After carbonization, the Raman spectrum is consistent with that of low-temperature glassy carbon [Fig. 1(b)]. This is characterized by a broad double-peaked feature at approximately $1350\ \text{cm}^{-1}$ and $1560\ \text{cm}^{-1}$, which can be attributed to the D band and G band, respectively, arising from the presence of sp^2 hybridized carbon.^{17,18} Both peaks are broad, owing to the low temperature ($450\ ^\circ\text{C}$) of carbonization, limiting the level of graphitization.¹³

Previous carbon foams derived from melamine possessed a bulk conductivity of just $6.8 \times 10^{-2}\ \text{S}/\text{cm}$ after carbonization at $1000\ ^\circ\text{C}$, only rising to $2.1\ \text{S}/\text{cm}^{-1}$ at a temperature of $1800\ ^\circ\text{C}$.¹² Here, we investigate the use of this carbon network as a carbon

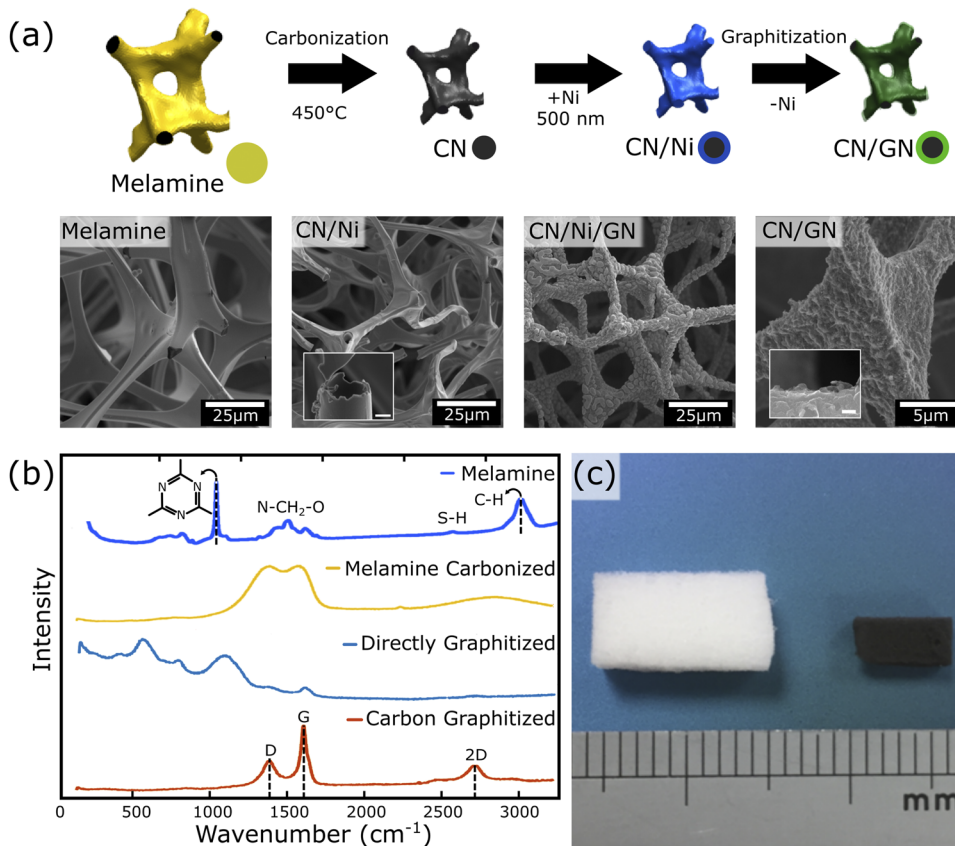


FIG. 1. (a) Schematic and associated SEM images for the shrinkage and subsequent conversion of melamine foams to a graphenic network (inset scale bars $1\ \mu\text{m}$). Commercial melamine foams are thermally converted to an identically shaped carbonaceous network with an $8\times$ decrease in volume. This shrunken template was used as the structure on which a thin catalytic layer of Ni was deposited electrolessly, onto which graphene layers are grown. Removal of Ni catalyst leaves behind a textured graphitic layer supported by the glassy carbon network beneath. (b) Raman spectra of pristine melamine foam display characteristic vibrational signatures containing ring bending ($500\text{--}800\ \text{cm}^{-1}$), triazine ring breathing ($975\ \text{cm}^{-1}$), N-CH₂-O group vibrations ($1250\text{--}1600\ \text{cm}^{-1}$), trace S-H vibrations ($2500\ \text{cm}^{-1}$), and strong C-H stretching ($3000\ \text{cm}^{-1}$). Thermally pre-treated samples developed characteristic multilayer graphitic Raman signatures, whereas the untreated template did not. (c) Optical images of the melamine foam before and after processing, illustrating the dramatic reduction in volume and change in color after carbonization.

source for subsequent catalytic graphitization and growth of a continuous graphitic network. For this, a conformal 500 nm thick layer of Ni was electrolessly deposited, as shown in the inset Fig. 1(a), which highlights the hollow coating around a broken strut. Samples first underwent an activating Pd pre-treatment before being immersed into a degassed (30 min, sonication) electroless Ni plating bath (Alfa Aesar) for a total of 10 min at 85 °C, with vigorous stirring. Ni-coated samples were then graphitized in a hot-walled CVD reactor at a temperature of 1065 °C for 90 min, under a 250 sccm flow of Ar at 50 mbar. After graphitization, islands of Ni are seen to form due to the Ni diffusion and de-wetting of the thin coating. Removal of the Ni catalyst was carried out using wet chemical etching in ammonium persulfate (0.2M) for 48 h. This results in a textured graphitic layer which is supported by the glassy carbon network beneath [Fig. 1(a)]. Ni diffusivity is prominent for the melamine foams, which can be attributed to the smooth surface post-shrinkage. SEM images taken at higher accelerating voltages reveal the continuous graphitic coating that surrounds the shrunken amorphous carbon skeleton, suggesting that graphitization occurs prior to significant catalyst diffusion [inset Fig. 1(a)]. As a control experiment, the direct catalytic graphitization of the untreated melamine foam was carried out with the same process and was found to be unsuccessful [Fig. 1(b)]. This is likely due to the disruption of the Ni coating by the decomposing polymer, as well as the strong presence of non-carbon elemental species in the melamine resin, which leach out during the carbonization process and are taken up by the Ni layer, poisoning the catalytic effect on graphene nucleation and growth. We note that graphene foams prepared from macroscopic templates typically require the use of a PMMA scaffold during

template removal, or the use of critical point drying, due to the effect of capillary forces that otherwise would lead to a collapse of the foam.⁷ Here, on the other hand, the presence of the amorphous carbon backbone allows for the 3D cellular geometry of the graphitic layers to be well preserved during the Ni removal, and no additional stabilization is required.

In comparison with stochastic foams, ordered lattice materials can be significantly more weight-efficient due to improved load distribution and stress transfer behavior throughout the lattice.^{19,20} Furthermore, control over pore size and cell structure can enhance the surface area and influence the tortuosity of fluid flow through the porous media.²¹ To demonstrate the applicability of our shrinkage and conversion method to ordered materials, a commercially printed 3D cubic lattice (Fig. 2) is processed in an equivalent way as outlined above. SLA printed resin formulations, as used herein, commonly utilize radical photoinitiators combined with acrylate-based monomers, each of which differs depending on the proprietary design of the resin.²² Cubic lattice samples were converted to an identically shaped carbonaceous network with 125× decrease in volume through the slow carbonization process, reducing the unit cell size from 1000 μm to 170 μm and strut widths from 550 μm to 65 μm (Fig. 3). The more dramatic reduction in volume compared to Fig. 1 is accompanied by an increase in mass loss to over 95%, owing to a larger fraction of degassed material.²³ The characteristic Raman spectra of the untreated resin can be seen in Fig. 2(b). The strong peak at approximately 2940 cm⁻¹ can be attributed to C–H stretching, arising from CH, CH₂, and CH₃ groups in a diverse range of side chains and microenvironments. After carbonization at 450 °C, the spectroscopic signatures show a nearly identical pyrolytic

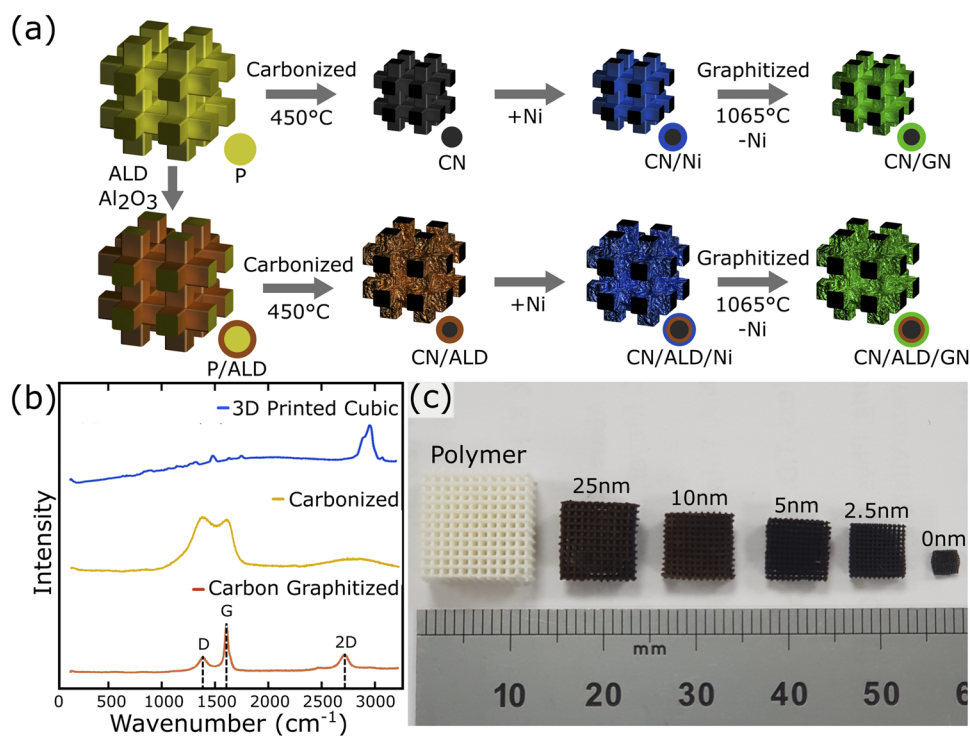


FIG. 2. (a) Schematic for the shrinkage and conversion of a polymeric lattice to graphenic network. Commercial polymeric foams are thermally converted to an identically shaped carbonaceous network with up to 125× decrease in volume. This shrunken template was used as the structure on which a thin catalytic layer of Ni was deposited electrolessly, onto which graphene layers are grown by means of pyrolysis. Ni templates were then removed by means of wet chemical etching. (b) Representative Raman spectra taken on samples as labeled. Pre-carbonized samples developed a characteristic multilayer graphitic Raman signature. The untreated template suffered a complete loss of order during the slow anneal phase. (c) Optical images demonstrating an 80% shrinkage in each direction occurs after process completion resulting in an over 125× reduction in volume. Addition of a 25 nm, 10 nm, 5 nm, or 2.5 nm thick ALD layer allows for the attenuation of the shrinkage and development of surface wrinkling (ALD thicknesses shown from left to right).

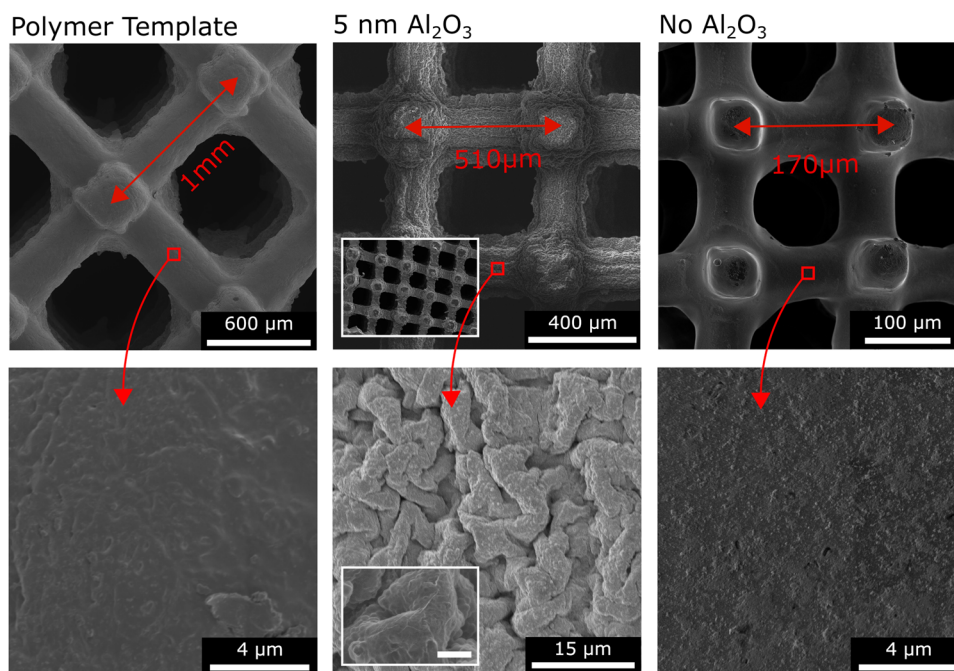


FIG. 3. SEM images of an ALD-arrested shrinkage process applied to 3D printed cubic lattices. 3D printed lattices begin at 1 mm unit cell size, which shrinks down to 170 μm after carbonization without an additional ALD layer, representing a $>5\times$ shrinkage in each lateral direction and an overall $>125\times$ reduction in volume. The addition of 5 nm of alumina by ALD results in reduced shrinkage and a pronounced wrinkling of the lattice surface. Low magnification inset shows large area isotropic shrinkage. High magnification inset shows the characteristic wrinkling of the graphene surface atop the pyrolytic carbon strut (inset scale bar 500 nm).

carbon spectrum as in Fig. 1, indicating the effectiveness of our process in removing non-carbon species. After plating of the Ni catalyst and further annealing, clear multilayer graphene signatures can be observed across the surface of the 3D lattice. The control experiment of processing a resin lattice without carbonization showed no such graphitization and was unstable during heating, leading to a loss of order. This is again likely due to a significant disruption of the Ni coating by the decomposing resin structure, which changes size considerably during carbonization.

In order to further control the shrinkage of the polymer template during carbonization, we employed ALD to add a thin conformal ceramic aluminum oxide (Al_2O_3) coating to the surface of the 3D printed resin. For this, we employed an ALD multi-pulse mode at 150 $^\circ\text{C}$, as described in detail elsewhere.²⁴ The use of a multi-pulse mode with extended exposure periods significantly improves the conformality of the Al_2O_3 coating on the resin lattice (Fig. 3), which was smooth before heating. When heated, a biaxial compressive stress is induced on the surface of the shrinking polymer. A stress mismatch between the shrinking polymer and alumina coating causes a pronounced wrinkling of the shrunken surface. The addition of a conformal layer of alumina also markedly influences the final shrink ratio of the carbonized template while remaining isotropic overall; see Figs. 2(c) and 3. A 2.5 nm alumina layer is found to reduce the shrink ratio of the cubic lattice to 9 \times , further decreasing down to 4 \times for a 25 nm thick alumina layer. In this way, the thickness of the added alumina layer can directly control the final surface roughness and surface area. The shrunken carbon/alumina network can then be used as a template to grow a thin graphitic film coating in an equivalent method to before, with carbon diffusion to the Ni catalyst occurring through cracks and holes in the ALD layer. The characteristic wrinkles of the as-grown graphene film can be seen in Fig. 3, encasing the surface of the strut.

Bulk foam resistivity was subsequently measured using a four-probe station (Keithley Model 4200-SCS) via the Van der Pauw method, with thickness taken as the apparent foam thickness as is standard in the literature.⁷ The bulk conductivity of the catalytically converted lattices was found to be 3.3 S/cm for the melamine precursor (Fig. 1) and ranges between 0.4 and 0.8 S/cm for the order resin precursor depending on the level of shrinkage (Fig. 2). In comparison, carbon foams formed by non-catalytic carbonization below 1100 $^\circ\text{C}$ remain non-conductive ($<6.8 \times 10^{-2}$ S/cm).¹² The conductivity of these graphitic microfoams is in line with graphene aerogels (0.1–1 S/cm)²⁵ while possessing reduced graphene loading, due to the improved conductivity of continuously bonded films compared to interconnected platelets.

Our results open a pathway to fabricating architected graphitic microfoams with the level of graphitization controlled by catalytic conversion and the cellular order controlled by 3D patterned polymeric templates. Dissimilar polymers are isotropically shrunken and converted to chemically equivalent carbonized templates, prior to further graphitization. We show that an ALD coating allows additional control of the shrinkage ratio and the introduction of surface wrinkling and higher surface area. Catalytic graphitization using a sacrificial Ni layer leads to the formation of a highly graphitized film present atop the strut surfaces, as evidenced by Raman spectra and enhanced conductivity of the structure. The shrinkage and conversion approach may be extended to alternative polymers, which may thermally degrade to form doped carbon²⁶ or ceramics,²⁷ which possess substantially varied physical properties.²⁸ Furthermore, the application of catalytically active nanomaterial coatings to the polymer pre- or post-shrinkage presents a facile pathway to a range of functional high surface area catalysts. The architected graphitic microfoams presented herein are promising for manifold

electrochemical or catalytic applications that require tuneable unit cell sizes, roughness, and conductivity.

The authors acknowledge funding from EPSRC (Grant No. EP/K016636/1, GRAPHTEd) and the ERC (Grant No. 279342, InsituNANO; Grant No. 669764, MULTILAT). K.N. acknowledges funding from the EPSRC Cambridge NanoDTC (Grant No. EP/G037221/1).

REFERENCES

- 1 M. T. Pettes, H. Ji, R. S. Ruoff, and L. Shi, "Thermal transport in three-dimensional foam architectures of few-layer graphene and ultrathin graphite," *Nano Lett.* **12**, 2959–2964 (2012).
- 2 J. Bauer, A. Schroer, R. Schwaiger, and O. Kraft, "Approaching theoretical strength in glassy carbon nanolattices," *Nat. Mater.* **15**, 438–443 (2016).
- 3 X. Dong *et al.*, "Hybrid structure of zinc oxide nanorods and three dimensional graphene foam for supercapacitor and electrochemical sensor applications," *RSC Adv.* **2**, 4364 (2012).
- 4 J. Bong *et al.*, "Dynamic graphene filters for selective gas-water-oil separation," *Sci. Rep.* **5**, 14321 (2015).
- 5 Z. Chen, C. Xu, C. Ma, W. Ren, and H. M. Cheng, "Lightweight and flexible graphene foam composites for high-performance electromagnetic interference shielding," *Adv. Mater.* **25**, 1296–1300 (2013).
- 6 Y. Dong, Z. S. Wu, W. Ren, H. M. Cheng, and X. Bao, "Graphene: A promising 2D material for electrochemical energy storage," *Sci. Bull.* **62**, 724–740 (2017).
- 7 Z. Chen *et al.*, "Three-dimensional flexible and conductive interconnected graphene networks grown by chemical vapour deposition," *Nat. Mater.* **10**, 424–428 (2011).
- 8 M. K. Alam and B. Maruyama, "Thermal conductivity of graphitic carbon foams," *Exp. Heat Transfer* **17**, 227–241 (2004).
- 9 S. Byun *et al.*, "Graphenes converted from polymers," *J. Phys. Chem. Lett.* **2**, 493–497 (2011).
- 10 B. Hu *et al.*, "Engineering carbon materials from the hydrothermal carbonization process of biomass," *Adv. Mater.* **22**, 813–828 (2010).
- 11 L. Sun *et al.*, "From coconut shell to porous graphene-like nanosheets for high-power supercapacitors," *J. Mater. Chem. A* **1**, 6462 (2013).
- 12 S. Chen *et al.*, "Elastic carbon foam via direct carbonization of polymer foam for flexible electrodes and organic chemical absorption," *Energy Environ. Sci.* **6**, 2435 (2013).
- 13 K. Jurkiewicz *et al.*, "Evolution of glassy carbon under heat treatment: Correlation structure-mechanical properties," *J. Mater. Sci.* **53**, 3509–3523 (2018).
- 14 X. Zhang, A. Vyatskikh, H. Gao, J. R. Greer, and X. Li, "Lightweight, flaw-tolerant, and ultrastrong nanoarchitected carbon," *Proc. Natl. Acad. Sci. U. S. A.* **116**, 6665–6672 (2019).
- 15 A. J. Jacobsen, S. Mahoney, W. B. Carter, and S. Nutt, "Vitreous carbon micro-lattice structures," *Carbon* **49**, 1025–1032 (2011).
- 16 A. V. Semenov, A. L. Pergament, and A. A. Pikalev, "Raman spectroscopy of melamine-formaldehyde resin microparticles exposed to processing in complex plasma," *J. Raman Spectrosc.* **47**, 1293–1297 (2016).
- 17 A. Ferrari and J. Robertson, "Interpretation of Raman spectra of disordered and amorphous carbon," *Phys. Rev. B* **61**, 14095–14107 (2000).
- 18 Z. Y. Chen *et al.*, "Observation of sp³ bonding in tetrahedral amorphous carbon using visible Raman spectroscopy," *J. Appl. Phys.* **88**, 2305 (2000).
- 19 L. J. Gibson and M. F. Ashby, "The mechanics of three-dimensional cellular materials," *Proc. R. Soc. A* **382**, 43–59 (1982).
- 20 J. R. Greer and V. S. Deshpande, "Three-dimensional architected materials and structures: Design, fabrication, and mechanical behavior," *MRS Bull.* **44**, 750–757 (2019).
- 21 P. Habisreuther, N. Djordjevic, and N. Zarzalis, "Statistical distribution of residence time and tortuosity of flow through open-cell foams," *Chem. Eng. Sci.* **64**, 4943–4954 (2009).
- 22 S. C. Ligon, R. Liska, J. Stampfl, M. Gurr, and R. Mühlaupt, "Polymers for 3D printing and customized additive manufacturing," *Chem. Rev.* **117**, 10212–10290 (2017).
- 23 B. Cardenas-Benitez *et al.*, "Pyrolysis-induced shrinking of three-dimensional structures fabricated by two-photon polymerization: Experiment and theoretical model," *Microsyst. Nanoeng.* **5**, 38 (2019).
- 24 A. I. Aria *et al.*, "Parameter space of atomic layer deposition of ultrathin oxides on graphene," *ACS Appl. Mater. Interfaces* **8**, 30564–30575 (2016).
- 25 S. Barg *et al.*, "Mesoscale assembly of chemically modified graphene into complex cellular networks," *Nat. Commun.* **5**, 4328 (2014).
- 26 J. P. Paraknowitsch, A. Thomas, and M. Antonietti, "A detailed view on the polycondensation of ionic liquid monomers towards nitrogen doped carbon materials," *J. Mater. Chem.* **20**, 6746–6758 (2010).
- 27 P. Colombo, "Mechanical properties of silicon oxycarbide ceramic foams," *J. Am. Ceram. Soc.* **51**, 2245–2251 (2004).
- 28 J. Yuan *et al.*, "Nitrogen-doped carbon fibers and membranes by carbonization of electrospun poly(ionic liquid)s," *Polym. Chem.* **2**, 1654–1657 (2011).